

Article

Cu(II) Coordination Polymers Containing Mixed Ligands with Different Flexibilities: Structural Diversity and Iodine Adsorption

 Shu-Yu Lin ¹, Yi-Lin Shen ¹, Wei-Hao Chen ¹, Manivannan Govindaraj ^{2,*}  and Jhy-Der Chen ^{1,*} 
¹ Department of Chemistry, Chung Yuan Christian University, Chung Li, Taoyuan City 320, Taiwan; kikimy123kikimy123@yahoo.com.tw (S.-Y.L.); lin740240@gmail.com (Y.-L.S.); a88q1127@gmail.com (W.-H.C.)

² Department of Chemistry, Periyar Maniammai Institute of Science & Technology (Deemed to be University), Vallam, Thanjavur 613 403, Tamil Nadu, India

* Correspondence: manivannang@pmu.edu (M.G.); jdchen@cycu.edu.tw (J.-D.C.); Tel.: +886-3-265-3351 (J.-D.C.)

Abstract: Reactions of *N,N'*-bis(3-methylpyridyl)oxalamide (**L**¹), *N,N'*-bis(3-methylpyridyl)adipoamide (**L**²) and *N,N'*-bis(3-methylpyridyl)sebacoamide (**L**³) with tricarboxylic acids and Cu(II) salts afforded {[Cu(**L**¹)(1,3,5-HBTC)]·H₂O}_n (1,3,5-H₃BTC = 1,3,5-benzenetricarboxylic acid), **1**, {[Cu_{1.5}(**L**²)_{1.5}(1,3,5-BTC)(H₂O)₂]·6.5H₂O}_n, **2**, [Cu(**L**²)_{0.5}(1,3,5-HBTB)]_n (1,3,5-H₃BTB = 1,3,5-tri(4-carboxyphenyl)benzene), **3**, [Cu₄(**L**³)(OH)₂(1,3,5-BTC)₂]_n, **4**, {[Cu₃(**L**³)₂(1,3,5-BTB)₂]·2.5MeOH·2H₂O}_n, **5**, and {[Cu₃(**L**³)₂(1,3,5-BTB)₂]·DMF·2H₂O}_n, **6**, which have been structurally characterized by using single crystal X-ray crystallography. Complexes **1–4** form a 2D layer with the {4⁴.6²}-**sqI** topology, a 2D layer with the (4.6²)₂(4².6².8²)-**bex** topology, a three-fold interpenetrated 3D net with the (4¹².6³)-**pcu** topology and a 3D framework with the (4¹⁰.6³².8³)(4².6)₂(4³.6³) topology, respectively, whereas **5** and **6** are 3D frameworks with the (6³)₂(6⁴.8²)(6⁸.8⁵.10²) topology. Complex **5** shows a better iodine adsorption factor of 290.0 mg g⁻¹ at 60 °C for 360 min than the other ones, revealing that the flexibility of the spacer ligand governs the structural diversity and the adsorption capacity.

Keywords: coordination polymer; crystal structure analysis; tricarboxylate; coordination mode



Citation: Lin, S.-Y.; Shen, Y.-L.; Chen, W.-H.; Govindaraj, M.; Chen, J.-D. Cu(II) Coordination Polymers Containing Mixed Ligands with Different Flexibilities: Structural Diversity and Iodine Adsorption. *Molecules* **2024**, *29*, 311. <https://doi.org/10.3390/molecules29020311>

Academic Editor: Jiafei Lyu

Received: 3 December 2023

Revised: 3 January 2024

Accepted: 3 January 2024

Published: 8 January 2024



Copyright: © 2024 by the authors. Licensee MDPI, Basel, Switzerland. This article is an open access article distributed under the terms and conditions of the Creative Commons Attribution (CC BY) license (<https://creativecommons.org/licenses/by/4.0/>).

1. Introduction

Coordination polymers (CPs) have shown crucial applications in many different areas due to their diverse structures and variable functions [1–8]. CPs can be constructed by the coordination of the designable spacer ligands to the metal ions, and through the self-assembly process, one- (1D), two- (2D) or three-dimensional (3D) network structures can be prepared.

The -(CH₂)_n- group of the bis-pyridyl-bis-amide (bpba) possesses suitable flexibility that may adopt the coordination environment of different metal ions, whereas the two amide groups play important roles as abundant potential hydrogen bond sites, affording CPs with remarkable topologies. On the other hand, polycarboxylate ligands that show distinct coordination modes involving chelating and bridging are also important in the organization of CPs in a mixed system [9]. Benzene-1,3,5-tricarboxylic acid (1,3,5-H₃BTC) is a planar molecule with C₃-symmetry that may give anions of the types, BTC³⁻ and HBTC²⁻, and intriguing structural types have been found in the bpba-based CPs supported by these anions [10]. Extension of 1,3,5-H₃BTC to the larger 1,3,5-tri(4-carboxyphenyl)benzene (1,3,5-H₃BTB) may thus afford CPs with different structural topology.

We are dedicated to illuminate the factors that may direct the structural diversity and govern the adsorption property of the flexible bpba-based CPs by exploring the variations in ligand conformation and coordination mode of the spacer ligands. In this study, flexible *N,N'*-bis(3-pyridylmethyl)oxalamide (**L**¹), *N,N'*-bis(3-methylpyridyl)adipoamide (**L**²) and *N,N'*-bis(3-methylpyridyl)sebacoamide (**L**³), Figure 1, were reacted with the Cu(II) metal salts and the tricarboxylic acids, 1,3,5-H₃BTC, and 1,3,5-H₃BTB, Figure 2,

to yield $\{[\text{Cu}(\text{L}^1)(1,3,5\text{-HBTC})]\cdot\text{H}_2\text{O}\}_n$ (1,3,5-H₃BTC = 1,3,5-benzenetricarboxylic acid), **1**, $\{[\text{Cu}_{1.5}(\text{L}^2)_{1.5}(1,3,5\text{-BTC})(\text{H}_2\text{O})_2]\cdot 6.5\text{H}_2\text{O}\}_n$, **2**, $[\text{Cu}(\text{L}^2)_{0.5}(1,3,5\text{-HBTB})]_n$ (1,3,5-H₃BTB = 1,3,5-tri(4-carboxyphenyl)benzene), **3**, $[\text{Cu}_4(\text{L}^3)(\text{OH})_2(1,3,5\text{-BTC})_2]_n$, **4**, $\{[\text{Cu}_3(\text{L}^3)_2(1,3,5\text{-BTB})_2]\cdot 2.5\text{MeOH}\cdot 2\text{H}_2\text{O}\}_n$, **5**, and $\{[\text{Cu}_3(\text{L}^3)_2(1,3,5\text{-BTB})_2]\cdot \text{DMF}\cdot 2\text{H}_2\text{O}\}_n$, **6**. The synthesis and structures of 1–6 as well as their iodine adsorptions form the subject of this report.

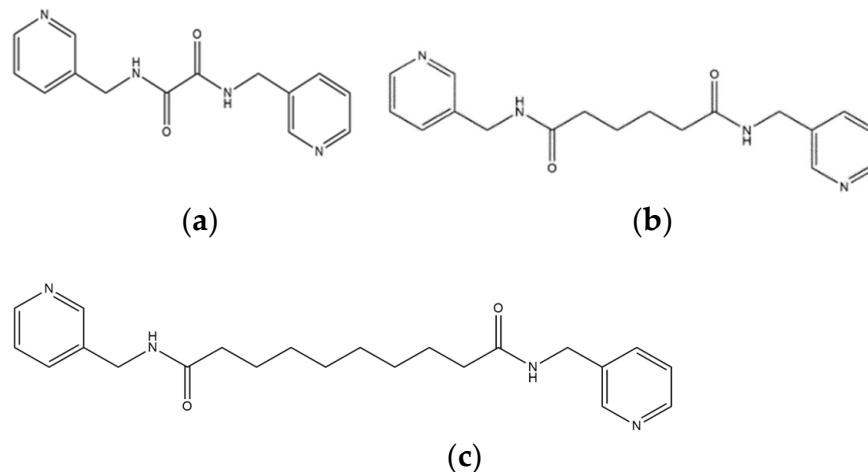


Figure 1. Structures of (a) L^1 , (b) L^2 and (c) L^3 .

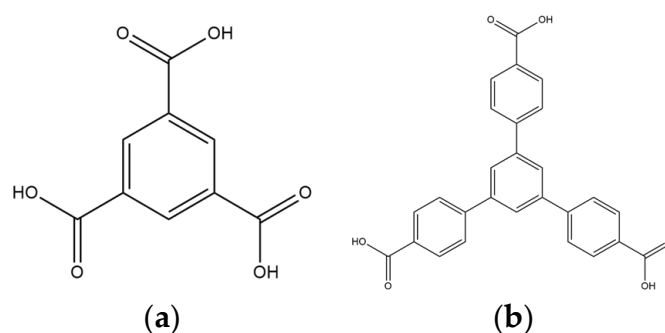


Figure 2. Structures of (a) 1,3,5-H₃BTC and (b) 1,3,5-H₃BTB.

2. Results and Discussion

2.1. Structure of **1**

A single-crystal X-ray diffraction analysis shows that complex **1** crystallizes in the triclinic space group $P\bar{1}$. There is one Cu(II) cation, one L^1 ligand, one 1,3,5-HBTC²⁻ ligand and one co-crystallized water molecule in the asymmetric unit. The Cu(II) cation is coordinated by two nitrogen atoms from L^1 ligands [Cu–N = 2.001(3)–2.007(3) Å] and three oxygen atoms from three 1,3,5-HBTC²⁻ ligands [Cu–O = 1.966(3)–2.237(3) Å], resulting in a trigonal bipyramidal geometry, and a dicopper unit is bridged by the 1,3,5-HBTC²⁻ ligands, Figure 3a. The Cu(II) cations are linked together by 1,3,5-HBTC²⁻ and L^1 ligands to afford a 2D structure. If the 1,3,5-HBTC²⁻ ligands are considered as three-connected nodes and the Cu(II) cations as five-connected nodes, the structure of **1** can be simplified as a 3,5-connected binodal 2D net with $(4^2\cdot 6^7\cdot 8)(4^2\cdot 6)\text{-}3,5\text{L}2$ topology (standard representation), Figure 3b, determined by using ToposPro program [11]. If the dinuclear Cu(II) units are defined as four connected nodes, the structure can be simplified as a four-connected net with $(4^4\cdot 6^2)\text{-sq1}$ topology (cluster representation), Figure 3c.

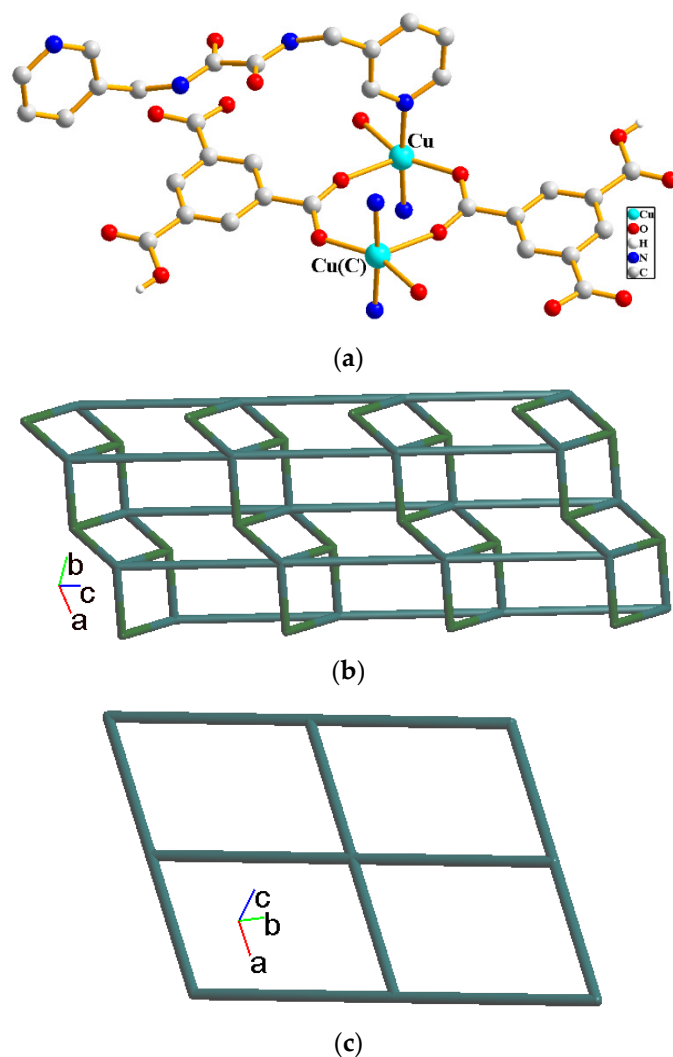


Figure 3. (a) Coordination environments of the Cu(II) cation in **1**. Symmetry transformations used to generate equivalent atoms: (C) $-x + 1, -y + 2$ and $-z + 1$. (b) A drawing showing the 2D net with $(4^2 \cdot 6^7 \cdot 8)(4^2 \cdot 6)-3,5L2$ topology. (c) A drawing showing the 2D net with $(4^4 \cdot 6^2)\text{-sql}$ topology.

2.2. Structure of **2**

The crystals of complex **2** conform to the triclinic space group $P\bar{1}$ and each asymmetric unit consists of two Cu(II) cations, one and a half L^2 ligands, one 1,3,5-BTC³⁻ ligand, two coordinated water molecules, and six and a half of a co-crystallized water molecules. The Cu(1) and Cu(2) metal centers are four- and five-coordinated, respectively, Figure 4a. While the Cu(1) atom is coordinated by two nitrogen atoms from the L^2 ligand [Cu-N = 2.051(2) Å] and two oxygen atoms from two 1,3,5-BTC³⁻ ligands [Cu-O = 1.960(2) Å], resulting in a distorted square geometry, the Cu(2) atom is coordinated by two nitrogen atoms from two L^2 ligands [Cu-N = 2.000(3)–2.006(3) Å], one oxygen atom from the 1,3,5-BTC³⁻ ligand [Cu-O = 1.978(2) Å] and two oxygen atoms from two coordinated water molecules [Cu-O = 2.023(2)–2.200(2) Å], giving a square pyramidal geometry. The Cu(II) cations are linked together by the 1,3,5-BTC³⁻ and L^2 ligands to afford a 2D layer. If the Cu(1) cations are defined as four-connected nodes and Cu(2) cations as three-connected nodes, the structure can be simplified as a 3,4-connected 2D net with $(4 \cdot 6^2)_2(4^2 \cdot 6^2 \cdot 8^2)\text{-bex}$ topology, Figure 4b.

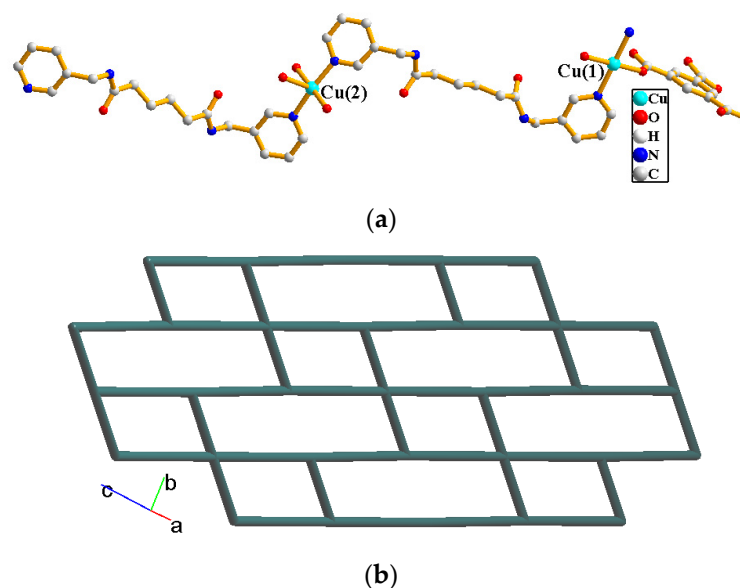


Figure 4. (a) Coordination environment of Cu(II) cations in **2**. (b) A drawing showing the 2D net with $(4.6^2)_2(4^2.6^2.8^2)$ -bex topology.

2.3. Structure of **3**

Complex **3** crystallizes in the monoclinic space group $C2/c$, and the asymmetric unit comprises one Cu(II) cation, a half of an L^2 ligand and one $1,3,5\text{-HBTB}^{2-}$ ligand. The Cu(II) cation is coordinated by one nitrogen atom from the L^2 ligand [Cu-N = 2.170(2) Å] and four oxygen atoms from four $1,3,5\text{-HBTB}^{2-}$ ligands [Cu-O = 1.9623(19)–1.9763(18) Å], resulting in a distorted square pyramidal geometry, Figure 5a. Two Cu(II) cations are bridged by the $1,3,5\text{-HBTB}^{2-}$ ligand to form a dinuclear unit with a Cu–Cu distance of 2.6516(6) Å that is shorter than the sum of two van der Waals radius of Cu (2.8 Å), suggesting the presence of weak intermolecular forces. The Cu(II) cations are linked together by $1,3,5\text{-HBTB}^{2-}$ and L^2 ligands to afford a 3D structure. If the dinuclear Cu(II) units are defined as six-connected nodes, the structure can be simplified as a six-connected net with $(4^{12}.6^3)$ -pcu topology, Figure 5b. The 3D nets penetrate into the neighbors to form a threefold 3D interpenetration structure, Figure 5c, demonstrating that the combination of the flexible L^2 and $1,3,5\text{-HBTB}^{2-}$ may lead to the formation of the entangled CP [12].

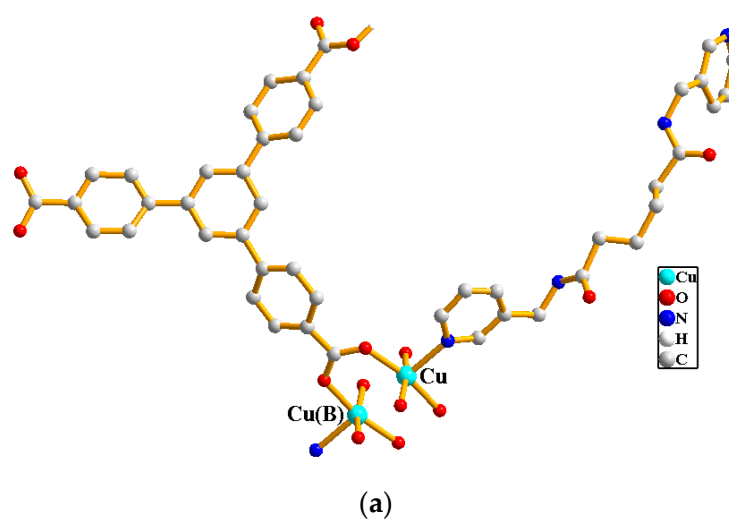


Figure 5. Cont.

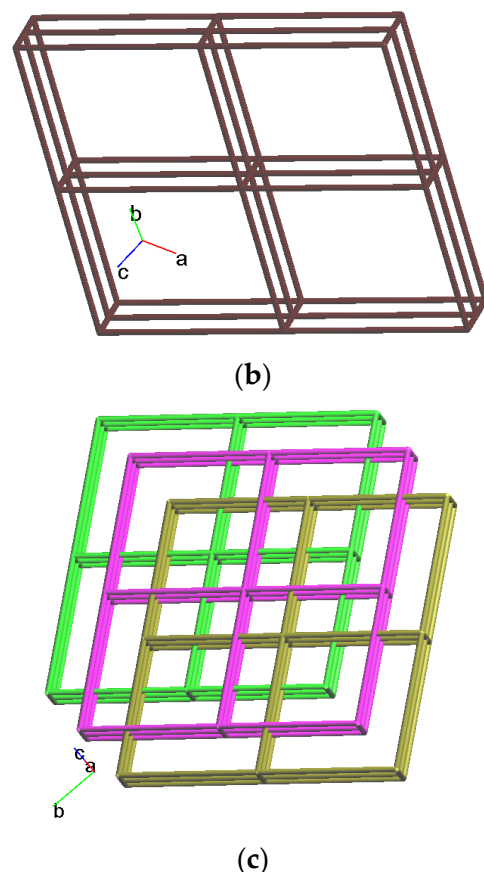


Figure 5. (a) Coordination environment of Cu(II) cations in **3**. Symmetry transformations used to generate equivalent atoms: (B) $-x + 1$, $-y + 1$ and $-z + 2$. (b) A drawing showing the structure with **pcu** topology. (c) A drawing showing the 3-fold interpenetrated net.

2.4. Structure of **4**

The crystals of complex **4** conform to the monoclinic space group $C2/c$. The asymmetric unit consists of two Cu(II) cations, a half of an L^3 ligand, one 1,3,5-BTC³⁻ ligand and one hydroxide ion. Figure 6a depicts the coordination environments of the Cu(II) cations. The Cu(1) and Cu(1B) atoms are symmetrically related by the inversion center, and each atom is coordinated by one oxygen atom from the L^3 ligand [Cu-O = 2.2720(16) Å], two oxygen atoms from two 1,3,5-BTC³⁻ ligands [Cu-O = 1.9377(14)–1.9434(14) Å] and two oxygen atoms from two hydroxy groups [Cu-O = 1.9551(13)–1.9620(13) Å], forming the square pyramidal geometry. On the other hand, each of the Cu(2) and Cu(2B) atoms is coordinated by one nitrogen atom from the L^3 ligand [Cu-N = 2.0164(17) Å], three oxygen atoms from three 1,3,5-BTC³⁻ ligands [Cu-O = 1.9473(13)–2.2909(15) Å] and one oxygen atom from the hydroxy group [Cu-O = 1.9482(13) Å], resulting in a distorted pentagonal bipyramidal geometry. The Cu(II) cations are linked together by 1,3,5-BTC³⁻ and L^3 ligands to afford a 3D structure. If the tetranuclear Cu(II) units are defined as ten-connected nodes, 1,3,5-BTC³⁻ ligands as three-connected nodes and L^3 as four-connected nodes, the structure can be simplified as a 3,4,10-connected trinodal net with the point symbol of $(4^{10} \cdot 6^{32} \cdot 8^3)(4^2 \cdot 6)_2(4^3 \cdot 6^3)$ topology, Figure 6b.

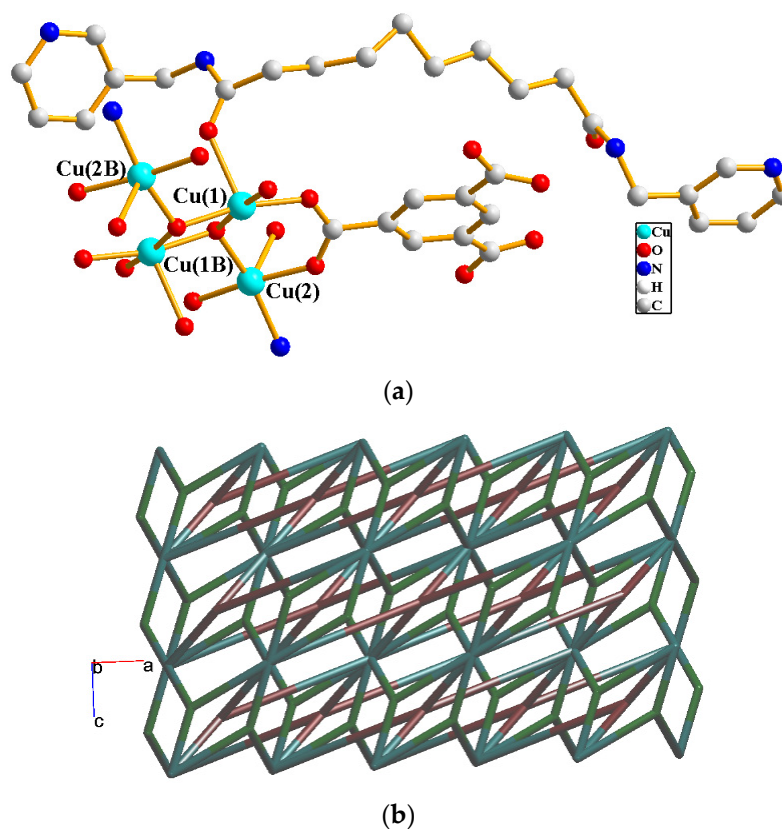


Figure 6. (a) Coordination environment of Cu(II) cations in **4**. Symmetry transformations used to generate equivalent atoms: (B) $-x + 3/2$, $-y + 3/2$ and $-z + 1$. (b) A drawing showing the 3D framework with $(4^{10} \cdot 6^{32} \cdot 8^3)(4^2 \cdot 6)_2(4^3 \cdot 6^3)$ topology.

2.5. Structure of **5** and **6**

Complexes **5** and **6** crystallize in the orthorhombic space group $Pna2_1$. Each of the asymmetric units of **5** and **6** comprise three Cu(II) cations, two L^3 ligands and two $1,3,5\text{-BTB}^{3-}$ ligands, with an additional two and a half co-crystallized methanol molecules and two co-crystallized water molecules in **5**, and two co-crystallized DMF molecules and two co-crystallized water molecules in **6**, respectively. Figure 7a shows the coordination environments of the Cu(II) cations in **5**. While the Cu(1) atom is coordinated by one nitrogen atom from the L^3 ligand [Cu(1)-N = 2.164(6) Å] and four oxygen atoms from four $1,3,5\text{-BTB}^{3-}$ ligands [Cu-O = 1.940(4)–2.005(4) Å], the Cu(2) atom is coordinated by one nitrogen atom from the L^3 ligand [Cu(2)-N = 2.189(6) Å] and four oxygen atoms from four $1,3,5\text{-BTB}^{3-}$ ligands [Cu-O = 1.933(5)–2.189(6) Å], resulting in square pyramidal geometries of both of the Cu(1) and Cu(2) atoms. The Cu(1) and Cu(2) atoms are bridged by the $1,3,5\text{-BTB}^{3-}$ ligands to form a dinuclear unit with a Cu---Cu distance of 2.6843(9) Å, indicating the presence of weak intermolecular forces. The Cu(3) atom is coordinated by two nitrogen atoms from two L^3 ligands [Cu-N = 2.054(7) and 2.079(7) Å] and two oxygen atoms from two $1,3,5\text{-BTB}^{3-}$ ligands [Cu-O = 1.913(6) and 1.917(5) Å], displaying a distorted square planar geometry.

Figure 7b shows the coordination environments of the Cu(II) cations in **6**. The Cu(1) atom is coordinated by two nitrogen atoms from the L^3 ligand [Cu-N = 2.027(6) and 2.034(6) Å] and two oxygen atoms from two $1,3,5\text{-BTB}^{3-}$ ligands [Cu-O = 1.918(5) and 1.941(5) Å], resulting in a distorted square planar geometry. Each of the Cu(2) and Cu(3) atoms is coordinated by one nitrogen atom from the L^3 ligand [Cu(2)-N = 2.183(5) Å; Cu(3)-N = 2.181(6) Å] and four oxygen atoms from four $1,3,5\text{-BTB}^{3-}$ ligands [Cu(2)-O = 1.929(4)–1.987(4) Å; Cu(3)-O = 1.929(4)–2.016(4) Å], resulting in square pyramidal geometries for Cu(2) and Cu(3). The Cu---Cu distance of 2.6922(9) Å between Cu(2) and Cu(3) is longer than that in complex **5**, indicating that the Cu(II)---Cu(II) interaction is subject to the

nature of the co-crystallized solvent molecules. The Cu(II) cations in **5** and **6** are linked together by 1,3,5-BTB³⁻ and L³ ligands to afford 3D structures. If the dinuclear Cu(II) units are defined as six-connected nodes, the mononuclear cations as four-connected nodes and 1,3,5-BTB³⁻ as three-connected nodes, while the L³ ligands are defined as linkers, the structures of **5** and **6** can be simplified as 3,4,6-connected 3D nets with the point symbol $(6^3)_2(6^4 \cdot 8^2)(6^8 \cdot 8^5 \cdot 10^2)$, Figure 7c.

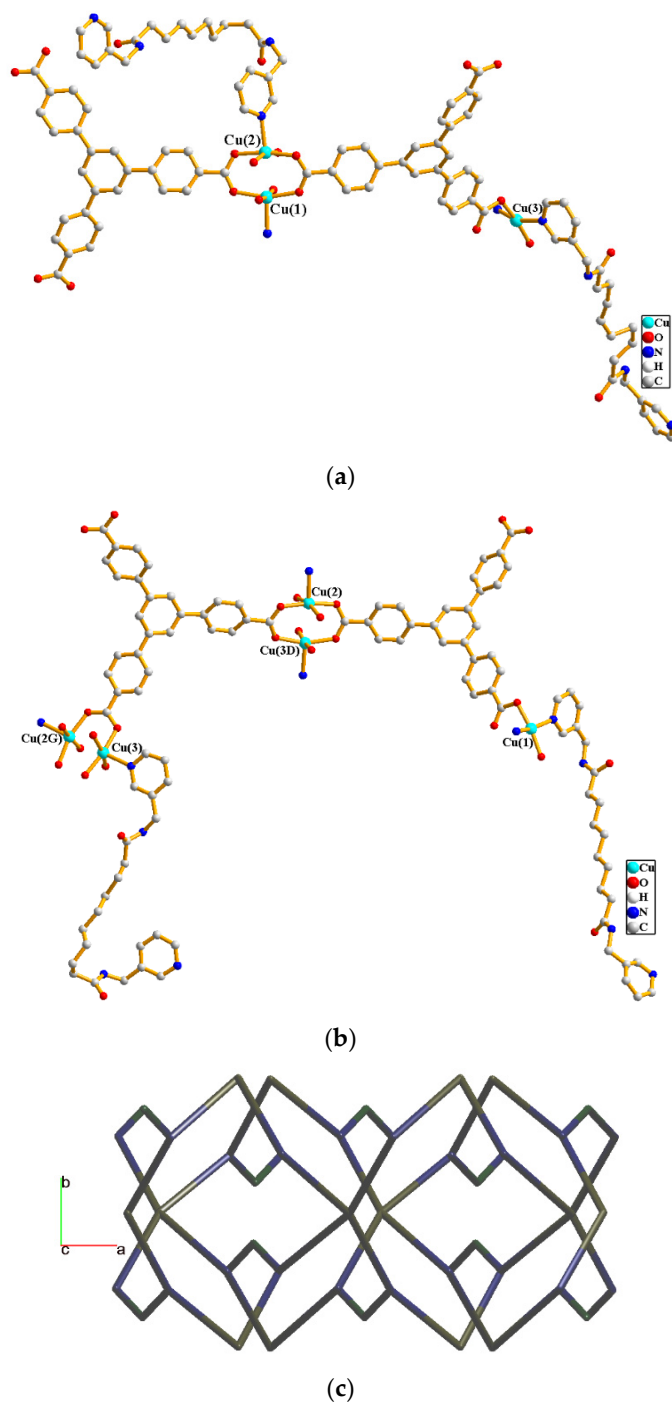


Figure 7. (a) Coordination environments of Cu(II) cations in **5**. (b) Coordination environments of Cu(II) cations in **6**. Symmetry transformations used to generate equivalent atoms: (D) $x + 1/2$, $-y + 1/2$ and z ; (G) $x - 1/2$, $-y + 1/2$ and z . (c) A drawing showing the 3,4,6-connected net with the point symbol $(6^3)_2(6^4 \cdot 8^2)(6^8 \cdot 8^5 \cdot 10^2)$.

2.6. Ligand Conformations and Coordination Modes

The ligand conformations of the bpba ligands have been proposed based on the torsion angles (θ) of their methylene carbon atoms [$0 \leq \theta \leq 90^\circ$, gauche (G), and $90 < \theta \leq 180^\circ$, anti (A)]. On the other hand, *cis* and *trans* are given if the two C=O groups are in the same and opposite directions, respectively. Three orientations, *syn-syn*, *syn-anti* and *anti-anti*, are also defined based on the relative position of pyridyl nitrogen and amide oxygen atoms. Accordingly, the ligand conformations of L¹–L³ in 1–6 are listed in Table 1. It is also noted that while the bpba ligands in 1, 2, 3, 5 and 6 bridge two Cu(II) cations through the two pyridyl nitrogen atoms, those in 4 bridge four Cu(II) cations through two pyridyl nitrogen and two amide oxygen atoms. Noticeably, although complexes 5 and 6 adopt the same structural type, the ligand conformations of the L³ ligands are significantly different, presumably due to the difference in the co-crystallized solvents. Moreover, the tricarboxylate ligands in 1–6 bridge two to five Cu(II) cations through various coordination modes, which are also listed in Table 1.

Table 1. Ligand conformations and bonding modes of complexes 1–6.

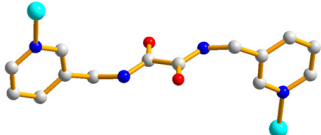
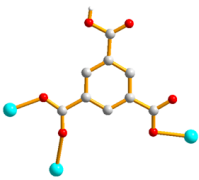
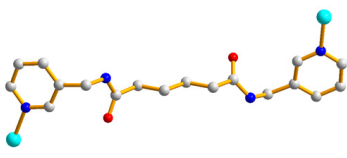
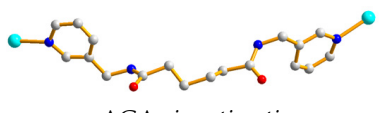
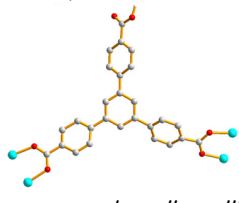
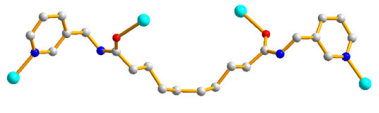
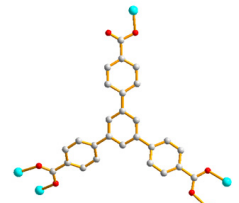
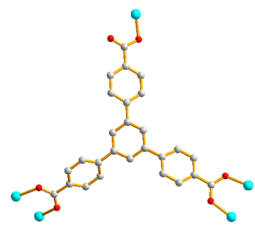
	Ligand Conformation	Coordination Mode
1	 <i>trans syn-syn</i>	 $\mu_3\text{-}\kappa\text{O}:\kappa\text{O}':\kappa\text{O}''$
2	 <i>AAA trans syn-syn</i>	 $\mu_2\text{-}\kappa\text{O}:\kappa\text{O}'$
3	 <i>AGA cis anti-anti</i>	 $\mu_4\text{-}\kappa\text{O}:\kappa\text{O}':\kappa\text{O}'':\kappa\text{O}'''$
4	 <i>AAAAAA cis anti-anti</i>	 $\mu_5\text{-}\kappa\text{O}:\kappa\text{O}':\text{O}'':\text{O}''':\text{O}''''$
5	 <i>GGAAAAA cis syn-syn</i>	 $\mu_5\text{-}\kappa\text{O}:\kappa\text{O}':\text{O}'':\text{O}''':\text{O}''''$

Table 1. Cont.

	Ligand Conformation	Coordination Mode
6	 AAAAAAA <i>trans anti-anti</i>	 $\mu_5\text{-}\kappa\text{O}:\kappa\text{O}':\text{O}'':\text{O}''':\text{O}''''$

2.7. Powder X-ray Analysis

In order to check the phase purity of the products, powder X-ray diffraction (PXRD) experiments were carried out for all complexes. As shown in Figures S7–S12, the peak positions of the experimental and simulated PXRD patterns are in agreement with each other, which demonstrates that the crystal structures are truly representative of the bulk materials. The differences in intensity may be owing to the preferred orientation of the powder samples.

2.8. Thermal Properties

Thermal gravimetric analysis (TGA) was carried out to examine the thermal decomposition from 30 to 800 or 900 °C. The samples were heated in nitrogen gas at a pressure of 1 atm with heating rate of 10 °C min⁻¹, and heating finished at 800 °C or 900 °C, Table 2, Figures S13–S18 indicate that complexes 1–6 display two-step weight loss involving a loss of solvent and a loss of organic ligands on heating.

Table 2. Thermal properties of complexes 1–6.

Complex	Weight Loss of Solvent °C (Calc/Found), %	Weight Loss of Ligand °C (Calc/Found), %
1	H ₂ O 30–250 (3.21/4.38)	L ¹ + 1,3,5-HBTC ²⁻ 250–800 (85.14/85.15)
2	6.5 H ₂ O 30–120 (16.19/14.38)	1.5 (L ²) + 1,3,5-BTC ³⁻ 120–900 (73.64/70.97)
3	0.5 DMA + 3 H ₂ O 30–250 (12.83/7.86)	0.5 (L ²) + 1,3,5-HBTB ²⁻ 250–800 (78.75/81.97)
4	-	L ³ + 2 (1,3,5-BTC ³⁻) + 2 (OH ⁻) 270–800 (76.50/80.31)
5	2.5 MeOH + 2 H ₂ O 30–270 (5.97/4.28)	2 (L ³) + 2 (1,3,5-BTB ³⁻) 270–800 (84.12/85.60)
6	DMF + H ₂ O 30–250 (4.71/6.03)	2 (L ³) + 2 (1,3,5-BTB ³⁻) 250–800 (84.42/84.54)

2.9. Iodine Adsorption

Radioactive iodine such as ¹²⁹I represents one of the most critical nuclear wastes which is harmful to human health and has to be captured and disposed of effectively [13–15]. On the other hand, CPs possessing porous structures may facilitate iodine adsorption through noncovalent interactions involving iodine and various sorption sites. Iodine adsorption experiments were thus carried out for complexes 1–6 to evaluate the degree of adsorption of iodine vapor at 25 and 60 °C within time intervals of 30, 60, 120, 180 and 360 min, respectively. For each experiment, 10 mg of the complex was placed in a 4 mL sample bottle inside a 20 mL sample bottle containing 100 mg of iodine, which was then sealed and kept

in the oven. Each experiment was repeated three times and the results averaged. It can be found that the colors of the complexes are different at different temperatures and time intervals, Figures S19–S30.

Tables S1–S12 summarize the I₂ adsorption of 1–6, followed by the plots displaying iodine vapor adsorption rates. With the increase in temperature from 25 to 60 °C, the absorption rate of iodine also has a good increase for each complex, giving the best adsorption factor of 290.0 mg g⁻¹ at 60 °C for 360 min for 5. In order to confirm whether the structures of the iodine-adsorbed complexes remain unchanged, their powder X-ray diffraction (PXRD) patterns were measured. As shown in Figures S31–S42, most of the experimental patterns are consistent with the theoretical ones, but 2 at 60 °C for 30 and 60 min, and 5 and 6 at 60 °C for 60 min display some changes.

The ability of the CPs to adapt iodine molecules to the voids of the network structures may govern the iodine adsorption capacity [16–19]. The solvent accessible volumes calculated by using the PLATON program [20] for 1–6 were 1.5, 17.3, 34.4, 2.9, 11.8 and 10.4%, respectively, of the unit cell volume, indicating that complex 3, which displays the three-fold interpenetrated 3D net with (4¹²·6³)-**pcu** topology, may accommodate more iodine than the other complexes. However, the best adsorption factor of 290.0 mg g⁻¹ at 60 °C for 360 min was observed for 5, demonstrating the important role of the flexibility of the neutral spacer ligands, L¹, L² and L³, in determining the iodine adsorption capacities of 1–6. The 3D framework of 5 containing the flexible L³ may be more susceptible to the changes in the ligand conformation upon the attack of the iodine molecules and thus may be more appropriate to accommodate the iodine molecules, which can probably be verified by the subtle change in the PXRD pattern of 5, Figure S40, upon iodine adsorption at 60 °C. On the other hand, the framework of the entangled 3 comprising L² is not vulnerable to the iodine attack, thus allowing for less iodine adsorption. The different performances in iodine adsorption between 5 and 6 are presumably due to the different co-crystallized solvents. The cavities of these complexes are small and thus most of the adsorptions are, as the reviewer suggested, due to surface uptakes.

We were not able to obtain the crystals suitable for single-crystal X-ray crystallography for the iodine-adsorbed samples. The iodine-adsorbed samples are usually anomalous, and energy dispersive X-ray (EDX) analysis was adopted to confirm iodine adsorption. The EDX experiments demonstrate the existence of the iodine atom rather than the identity of the iodine atom, *vide infra*. It has been reported that the iodine molecules can be transformed into anionic I₃⁻ or I₅⁻ in the iodine-adsorbed CPs [21]. Thus, it is not probable to determine whether the adsorption is reversible or irreversible at this moment.

Although the solvent accessible volumes (or the cavity sizes) of the CPs may govern such performances, the identities of the metal centers and the supporting ligands and stabilities of the CPs may also play important roles. The bpba ligands used in this report are well known for their amide groups that may interact with the incoming molecules through hydrogen bonds originating from the amine hydrogen atoms or the carbonyl oxygen atoms. By fixing the similar factors, we have shown that the best adsorption factor of 290.0 mg g⁻¹ at 60 °C for 360 min was observed for 5, demonstrating the important role of the flexibility of the neutral spacer ligands, L¹, L² and L³, in determining the iodine adsorption capacities of 1–6. For comparison, it is noted that the interpenetrated Th-SINAP-16 and Th-SINAP-21 appear to exhibit uptake amounts of 354 and 375 mg g⁻¹, respectively, after 0.5 h of iodine adsorption [21], whereas the Ni(II) CP {[Ni(L³)(OBA)(H₂O)₂]}·2H₂O_n encapsulates 166.55 mg g⁻¹ iodine at 60 °C [16].

2.10. Energy Dispersive X-ray (EDX) Analysis

EDX analyses were performed for complexes 1–6 after iodine adsorption to investigate their iodine uptakes, Figures S43–S48. Three positions of the iodine-adsorbed samples of complexes 1–6 were selected for each measurement, and the amount of iodine was different for each position, indicating the inhomogeneous distribution of iodine in the iodine-adsorbed samples.

2.11. Gas Adsorption

Low-pressure N₂ adsorption and desorption measurements were performed at 77 K for complexes 1–6, which were heated at 120 °C for 24 h to obtain fully activated samples before the measurements. Figures S49–S54 demonstrate that the complexes 1 and 3–6 remain stable upon the removal of the solvent molecules, while the structure of 2 has changed. The Brunauer–Emmet–Teller (BET) surface areas are 7.49, 13.60, 12.82, 12.60, 11.73 and 7.98 m²/g, and the N₂ uptake capacities are 6.93, 18.33, 12.70, 11.28, 10.83 and 8.12 cm³/g, respectively, for 1–6, Figures S55–S60, indicating larger surface area and N₂ uptake for 2 upon desolvation. Moreover, pore-sized distribution curves show that the pore sizes are 2.9, 3.4, 3.4, 3.7, 3.4 and 3.4 nm, respectively, for 1–6, Figures S61–S66.

As demonstrated by the experiments, the BET surface area and N₂ uptakes of 1–6 derived from the low-pressure N₂ adsorption and desorption measurements are not closely related to their iodine adsorption capacities. Therefore, the iodine adsorption capacity may also depend on the characteristics of the CPs and their surface features.

3. Materials and Methods

3.1. Materials

The reagent Cu(CH₃COO)₂·H₂O was purchased from Showa, 1,3,5-benzenetricarboxylic acid (1,3,5-H₃BTC) from Alfa Aesar and 1,3,5-tri(4-carboxyphenyl)benzene (1,3,5-H₃BTB) from Alfa Aesar. The ligands *N,N'*-bis(3-methylpyridyl)oxalamide (**L**¹), *N,N'*-bis(3-methylpyridyl)adipoamide (**L**²) and *N,N'*-bis(3-methylpyridyl)sebacoamide (**L**³) were prepared according to published procedures [22].

3.2. Preparations

3.2.1. {[Cu(**L**¹)(1,3,5-HBTC)]·H₂O}_n, **1**

A mixture of Cu(CH₃COO)₂·H₂O (0.020 g, 0.10 mmol), **L**¹ (0.027 g, 0.10 mmol) and 1,3,5-H₃BTC (0.021 g, 0.10 mmol) in 10 mL of H₂O was sealed in a 23 mL Teflon-lined steel autoclave, which was heated under autogenous pressure to 120 °C for two days, and then cooled down to room temperature for two days. Blue crystals suitable for single-crystal X-ray diffraction were obtained. Yield: 0.081 g (72%). Anal. Calcd for C₂₃H₂₀CuN₄O₉ (MW = 599.97): C, 49.33; N, 10.00; H, 3.60%. Found: C, 49.39; N, 9.85; H, 3.48%. FT-IR (cm⁻¹): 3313 (s), 2357 (m), 1621 (s), 1519 (m), 1430 (m), 1351 (s), 1099 (m), 860 (w), 756 (m), 609 (w) and 512 (w).

3.2.2. {[Cu_{1.5}(**L**²)_{1.5}(1,3,5-BTC)(H₂O)₂]·6.5H₂O}_n, **2**

Complex **2** was prepared by following similar procedures for **1**, except that Cu(CH₃COO)₂·H₂O (0.020 g, 0.10 mmol), **L**² (0.033 g, 0.10 mmol) and 1,3,5-H₃BTC (0.021 g, 0.10 mmol) in 10 mL of NaOH (0.01 M) aqueous solution were used, which was heated to 100 °C. Blue crystals were obtained. Yield: 0.054 g (86%). Anal. Calcd for C₃₆H₅₃Cu_{1.5}N₆O_{17.5} (MW = 945.15): C, 45.75; N, 8.89; H, 5.65%. Found: C, 46.19; N, 8.69; H, 5.62%. FT-IR (cm⁻¹): 3054 (m), 2359 (m), 1606 (s), 1427 (m), 1352 (s), 1196 (m), 1058 (w), 811 (w) and 710 (m).

3.2.3. [Cu(**L**²)_{0.5}(1,3,5-HBTB)]_n, **3**

Complex **3** was prepared by following similar procedures for **1**, except that Cu(CH₃COO)₂·H₂O (0.020 g, 0.10 mmol), **L**² (0.033 g, 0.10 mmol) and 1,3,5-H₃BTB (0.044 g, 0.10 mmol) in 7 mL of H₂O and 3 mL of DMA were used. Green crystals were obtained. Yield: 0.032 g (42%). Anal Calcd for C₃₆H₂₇CuN₂O₇ (MW = 663.13): C, 65.20; N, 4.22; H, 4.10%. Anal Calcd for C₃₆H₂₇CuN₂O₇·0.5DMA·3H₂O (MW = 760.72): C, 59.99; N, 4.60; H, 4.97%. Found: C, 59.94; N, 4.84; H, 4.73%. FT-IR (cm⁻¹): 2360 (m), 1604 (s), 1390 (s), 1176 (w), 1015 (m), 853 (w), 774 (s) and 669 (w).

3.2.4. $[\text{Cu}_4(\text{L}^3)(\text{OH})_2(1,3,5\text{-BTC})_2]_n$, **4**

Complex **4** was prepared by following similar procedures for **1**, except that $\text{Cu}(\text{CH}_3\text{COO})_2 \cdot \text{H}_2\text{O}$ (0.020 g, 0.10 mmol), L^3 (0.038 g, 0.10 mmol) and 1,3,5- H_3BTC (0.021 g, 0.10 mmol) in 10 mL of H_2O were used. Blue crystals were obtained. Yield: 0.016 g (60%). Anal. Calcd for $\text{C}_{40}\text{H}_{38}\text{Cu}_4\text{N}_4\text{O}_{16}$ (MW = 1084.90): C, 44.28; N, 5.16; H, 3.53%. Found: C, 44.49; N, 5.22; H, 3.87%. FT-IR (cm^{-1}): 3238 (m), 2363 (m), 1583 (s), 1442 (m), 1353 (s), 1094 (w), 761 (m), 716 (m) and 586 (w).

3.2.5. $\{[\text{Cu}_3(\text{L}^3)_2(1,3,5\text{-BTB})_2] \cdot 2.5\text{MeOH} \cdot 2\text{H}_2\text{O}\}_n$, **5**, and $\{[\text{Cu}_3(\text{L}^3)_2(1,3,5\text{-BTB})_2] \cdot \text{DMF} \cdot 2\text{H}_2\text{O}\}_n$, **6**

Complexes **5** and **6** were prepared by following similar procedures for **1** but in different solvent systems. While complex **5** was prepared from a reaction mixture of $\text{Cu}(\text{CH}_3\text{COO})_2 \cdot \text{H}_2\text{O}$ (0.020 g, 0.10 mmol), L^3 (0.038 g, 0.10 mmol) and 1,3,5- H_3BTB (0.044 g, 0.10 mmol) in 3 mL of H_2O and 7 mL of MeOH, complex **6** was obtained in 7 mL of H_2O and 3 mL of DMF. Green crystals were obtained for **5**. Yield: 0.018 g (28%). Anal. Calcd for $\text{C}_{100.50}\text{H}_{104}\text{Cu}_3\text{N}_8\text{O}_{20.50}$ (MW = 1942.53): C, 62.14; N, 5.77; H, 5.40%. Found: C, 61.93; N, 5.59; H, 4.86%. FT-IR (cm^{-1}): 3068 (m), 2925 (m), 2360 (w), 1596 (s), 1406 (s), 1179 (w), 1015 (w), 854 (w), 778 (m) and 700 (w). Green crystals were obtained for **6**. Yield: 0.036 g (56%). Anal. Calcd for $\text{C}_{101}\text{H}_{101}\text{Cu}_3\text{N}_9\text{O}_{19}$ (MW = 1935.52): C, 62.67; N, 6.51; H, 5.26%. Anal. Calcd for **6** + 3 H_2O , $\text{C}_{101}\text{H}_{107}\text{Cu}_3\text{N}_9\text{O}_{22}$ (MW = 1989.52): C, 60.97; N, 6.34; H, 5.42%. Found: C, 60.67; N, 6.33; H, 5.02%. FT-IR (cm^{-1}): 3065 (m), 2357 (w), 1599 (s), 1393 (s), 1177 (w), 1015 (m), 851 (m), 775 (s), 702 (m) and 668 (w).

The IR spectra of complexes **1–6** are provided as Figures S1–S6 in the Supplementary Materials.

3.3. X-ray Crystallography

A Bruker AXS SMART APEX II CCD diffractometer, equipped with a graphite-monochromated $\text{MoK}\alpha$ radiation (0.71073 Å), was used to collect diffraction data for complexes **1–6**. The diffraction data were then reduced by using standard methods [23], followed by empirical absorption corrections based on a “multi-scan”. The positions of some of the heavier atoms were located by the direct method or Patterson method, and the remaining atoms were found in a series of alternating difference Fourier maps and least-square refinements. The hydrogen atoms, except those of the water molecules, were added by using the HADD command in SHELXTL 6.1012 [24]. Due to the serious disordering, the solvent molecules in **3** were squeezed by using the PLATON program [20] and their diffraction data were reported without solvent contribution. Table 3 lists the crystal and structure refinement parameters for **1–6**. The CCDC no. 2311169–2311174 contains the supplementary crystallographic data for this paper. These data can be obtained free of charge via <http://www.ccdc.cam.ac.uk/conts/retrieving.html> or from the Cambridge Crystallographic Data Centre, 12 Union Road, Cambridge CB2 1EZ, UK; fax: +44 1223 336 033; e-mail: deposit@ccdc.cam.ac.uk; or at <http://www.ccdc.cam.ac.uk>.

Table 3. Crystal data for complexes **1–6**.

Complex	1	2	3
CCDC No.	2311169	2311170	2311171
Formula	$\text{C}_{23}\text{H}_{20}\text{CuN}_4\text{O}_9$	$\text{C}_{36}\text{H}_{53}\text{Cu}_{1.5}\text{N}_6\text{O}_{17.50}$	$\text{C}_{36}\text{H}_{27}\text{CuN}_2\text{O}_7$
Formula weight	599.97	945.15	663.13
Crystal system	Triclinic	Triclinic	Monoclinic
Space group	$P\bar{1}$	$P\bar{1}$	$C2/c$
a, Å	10.1482(9)	8.9062(2)	18.8531(6)
b, Å	11.1855(10)	11.2565(3)	25.8032(8)

Table 3. Cont.

Complex	1	2	3
c, Å	11.7055(11)	22.7418(5)	17.4503(6)
α , °	111.285(3)	99.7718(14)	90
β , °	97.429(3)	94.3827(15)	99.4362(19)
γ , °	108.425(3)	105.8728(14)	90
V, Å ³	1128.97(18)	2142.95(9)	8374.2(5)
Z	2	2	8
D _{calc} , Mg/m ³	1.647	1.465	1.052
F(000)	574	989	2736
μ (Mo K α), mm ⁻¹	1.032	0.831	0.561
Range(2 θ) for data collection, deg	3.88 ≤ 2 θ ≤ 51.99	3.66 ≤ 2 θ ≤ 56.62	3.34 ≤ 2 θ ≤ 56.62
Independent reflection	4415 [R(Int) = 0.0643]	10315 [R(Int) = 0.0539]	10067 [R(Int) = 0.0745]
Data/restraint/parameter	4415/0/338	10315/0/556	10067/0/432
quality-of-fit indicator ^c	1.054	1.015	0.990
Final R indices [I > 2 σ (I)] ^{a,b}	R ₁ = 0.0555, wR ₂ = 0.1419	R ₁ = 0.0550, wR ₂ = 0.1228	R ₁ = 0.0536, wR ₂ = 0.1164
R indices (all data)	R ₁ = 0.0755, wR ₂ = 0.1668	R ₁ = 0.1158, wR ₂ = 0.1452	R ₁ = 0.1022, wR ₂ = 0.1345
Complex	4	5	6
CCDC No.	2311172	2311173	2311174
Formula	C ₄₀ H ₃₈ Cu ₄ N ₄ O ₁₆	C _{100.50} H ₁₀₄ Cu ₃ N ₈ O _{20.50}	C ₁₀₁ H ₁₀₁ Cu ₃ N ₉ O ₁₉
Formula weight	1084.90	1942.53	1935.52
Crystal system	Monoclinic	Orthorhombic	Orthorhombic
Space group	C2/c	Pna2 ₁	Pna2 ₁
a, Å	16.5969(9)	20.9682(10)	22.0739(18)
b, Å	13.9067(4)	25.3489(11)	24.3392(18)
c, Å	17.6110(5)	18.1699(8)	17.9481(15)
α , °	90	90	90
β , °	90.2248(9)	90	90
γ , °	90	90	90
V, Å ³	4064.73(19)	9657.7(8)	9642.8(13)
Z	4	4	4
D _{calc} , Mg/m ³	1.773	1.336	1.333
F(000)	2200	4056	4036
μ (Mo K α), mm ⁻¹	2.145	0.728	0.728
Range (2 θ) for data collection, deg	3.82 ≤ 2 θ ≤ 56.59	2.75 ≤ 2 θ ≤ 51.99	2.82 ≤ 2 θ ≤ 56.63
Independent reflection	5049 [R(Int) = 0.0283]	18994 [R(Int) = 0.0510]	20288 [R(Int) = 0.0765]
Data/restraint/parameter	5049/0/311	18994/2119/1157	20288/1/1181

Table 3. Cont.

Complex	4	5	6
quality-of-fit indicator ^c	1.085	1.026	1.002
Final R indices [I > 2σ(I)] ^{a,b}	R ₁ = 0.0265, wR ₂ = 0.0690	R ₁ = 0.0526, wR ₂ = 0.1408	R ₁ = 0.0571, wR ₂ = 0.1019
R indices (all data)	R ₁ = 0.0323, wR ₂ = 0.0747	R ₁ = 0.0664, wR ₂ = 0.1503	R ₁ = 0.1364, wR ₂ = 0.1244

^a $R_1 = \sum ||F_o| - |F_c|| / \sum |F_o|$. ^b $wR_2 = [\sum w(F_o^2 - F_c^2)^2 / \sum w(F_o^2)^2]^{1/2}$. $w = 1 / [\sigma^2(F_o^2) + (ap)^2 + (bp)]$. $p = [\max(F_o^2 \text{ or } 0) + 2(F_c^2)] / 3$. $a = 0.1039$, $b = 1.1215$ for 1; $a = 0.0650$, $b = 0$ for 2; $a = 0.0585$, $b = 0$ for 3; $a = 0.0330$, $b = 9.2346$ for 4; $a = 0.0856$, $b = 10.2363$ for 5; $a = 0.0496$, $b = 0$ for 6. ^c quality of fit = $[\sum w(|F_o^2| - |F_c^2|)^2 / (N_{\text{observed}} - N_{\text{parameters}})]^{1/2}$.

4. Conclusions

Six new CPs supported by the mixed ligands with different flexibilities have been synthesized. Complexes 1–4 form a 2D layer with {4⁴.6²}-sql topology, a 2D layer with (4.6²)₂(4².6².8²)-bex topology, a three-fold interpenetrated 3D net with (4¹².6³)-pcu topology and a 3D net with (4¹⁰.6³².8³)(4².6)₂(4³.6³) topology, respectively, whereas 5 and 6 are 3D nets with the same (6³)₂(6⁴.8²)(6⁸.8⁵.10²) topology, showing that the use of the extended 1,3,5-H₃BTB afforded different structural types as compared with those derived from 1,3,5-H₃BTC, and a combination of the flexible L² with 1,3,5-H₃BTB gave an entangled CP. Among the six CPs, complex 5 reveals the best iodine adsorption capacity. This report offers an insight into understanding the roles of flexibility of the bpba and tricarboxylate ligands in determining the structural diversity as well as the iodine adsorption capacity.

Supplementary Materials: The following supporting information can be downloaded at: <https://www.mdpi.com/article/10.3390/molecules29020311/s1>.

Author Contributions: Investigation, S.-Y.L.; data curation, Y.-L.S. and W.-H.C.; review and supervision, M.G. and J.-D.C. All authors have read and agreed to the published version of the manuscript.

Funding: This research was funded by the National Science and Technology Council of the Republic of China: NSTC 112-2113-M-033-004.

Institutional Review Board Statement: Not applicable.

Informed Consent Statement: Not applicable.

Data Availability Statement: Data are contained within the article or Supplementary Materials.

Acknowledgments: We are grateful to the National Science and Technology Council of the Republic of China for support.

Conflicts of Interest: The authors declare no conflicts of interest.

References

- Tiekink, E.R.; Vittal, J.J. *Frontiers in Crystal Engineering*; John Wiley & Sons: West Sussex, UK, 2006.
- Batten, S.R.; Neville, S.M.; Turner, D.R. *Coordination Polymers Design, Analysis and Application*; The Royal Society of Chemistry: London, UK, 2009.
- Allendorf, M.D.; Bauer, C.A.; Bhakta, R.K.; Houk, R.J.T. Luminescent metal–organic frameworks. *Chem. Soc. Rev.* **2009**, *38*, 1330.
- Shi, Y.X.; Zhang, W.H.; Abrahams, B.F.; Braunstein, P.; Lang, J.P. Fabrication of Photoactuators: Macroscopic Photomechanical Responses of Metal–Organic Frameworks to Irradiation by UV Light. *Angew. Chem. Int. Ed.* **2019**, *58*, 9453–9458. [[CrossRef](#)] [[PubMed](#)]
- Shi, Y.X.; Chen, H.H.; Zhang, W.H.; Day, G.S.; Lang, J.P.; Zhou, H.C. Photoinduced nonlinear contraction behavior in metalorganic frameworks. *Chem. Eur. J.* **2019**, *25*, 8543–8549. [[CrossRef](#)]
- Liu, D.; Lang, J.-P.; Abrahams, B.F. Highly Efficient Separation of a Solid Mixture of Naphthalene and Anthracene by a Reusable Porous Metal–Organic Framework through a Single-Crystal-to-Single Crystal Transformation. *J. Am. Chem. Soc.* **2011**, *133*, 11042. [[CrossRef](#)]
- Liu, C.-Y.; Chen, X.-R.; Chen, H.-X.; Niu, Z.; Hirao, H.; Braunstein, P.; Lang, J.-P. Ultrafast Luminescent Light-Up Guest Detection Based on the Lock of the Host Molecular Vibration. *J. Am. Chem. Soc.* **2020**, *142*, 6690–6697. [[CrossRef](#)]

8. Manna, F.; Oggianu, M.; Avarvari, N.; Mercuri, M.L. Lanthanide-Based Metal–Organic Frameworks with Single-Molecule Magnet Properties. *Magnetochemistry* **2023**, *9*, 190.
9. Mondal, S.; Dastidar, P. Mixed Ligand Coordination Polymers for Metallogelation and Iodine Adsorption. *Cryst. Growth Des.* **2019**, *19*, 470–478. [[CrossRef](#)]
10. Chen, C.-J.; Chen, C.-L.; Lee, W.-T.; Hu, J.-H.; Chhetri, P.M.; Chen, J.-D. Coordination polymers with a semi-rigid spacer ligand in a mixed system: Roles of benzene-1, 3, 5-tricarboxylate anions. *J. Mol. Struct.* **2021**, *1244*, 131252. [[CrossRef](#)]
11. Blatov, V.A.; Shevchenko, A.P.; Proserpio, D.M. Applied topological analysis of crystal structures with the program package ToposPro. *Cryst. Growth Des.* **2014**, *14*, 3576–3586. [[CrossRef](#)]
12. Huang, W.-C.; Chen, W.-H.; Chen, C.-L.; Liao, T.-T.; Chen, Y.-W.; Chen, J.-D. Formation of entangled Co(II) coordination polymers based on bis-pyridyl-bis-amide and angular dicarboxylate ligands: A structural comparison. *CrystEngComm* **2023**, *25*, 5575–5587. [[CrossRef](#)]
13. Safarifard, V.; Morsali, A. Influence of an amine group on the highly efficient reversible adsorption of iodine in two novel isoreticular interpenetrated pillared-layer microporous metal–organic frameworks. *CrystEngComm*. **2014**, *16*, 8660–8663. [[CrossRef](#)]
14. Guo, B.; Li, F.; Wang, C.; Zhang, L.; Sun, D. A rare (3, 12)-connected zirconium metal–organic framework with efficient iodine adsorption capacity and pH sensing. *J. Mater. Chem. A* **2019**, *7*, 13173–13179. [[CrossRef](#)]
15. Arici, M.; Arici, T.A.; Demiral, H.; Taş, M.; Yeşilel, O.Z. A porous Zn (II)-coordination polymer based on a tetracarboxylic acid exhibiting selective CO₂ adsorption and iodine uptake. *Dalton Trans.* **2020**, *49*, 10824–10831. [[CrossRef](#)] [[PubMed](#)]
16. Lee, W.T.; Liao, T.T.; Chen, J.-D. Nickel (II) Coordination Polymers Supported by Bis-pyridyl-bis-amide and Angular Dicarboxylate Ligands: Role of Ligand Flexibility in Iodine Adsorption. *Int. J. Mol. Sci.* **2022**, *23*, 3603. [[CrossRef](#)] [[PubMed](#)]
17. Mohanambe, L.; Vasudevan, S. Insertion of iodine in a functionalized inorganic layered solid. *Inorg. Chem.* **2004**, *43*, 6421–6425. [[CrossRef](#)]
18. Zhang, N.; Sun, L.X.; Bai, F.Y.; Xing, Y.H. Thorium–organic framework constructed with a semirigid triazine hexacarboxylic acid ligand: Unique structure with thorium oxide wheel clusters and iodine adsorption behavior. *Inorg. Chem.* **2020**, *59*, 3964–3973. [[CrossRef](#)]
19. Liu, J.H.; Qi, Y.J.; Zhao, D.; Li, H.H.; Zheng, S.T. Heterometallic organic frameworks built from trinuclear indium and cuprous halide clusters: Ligand-oriented assemblies and iodine adsorption behavior. *Inorg. Chem.* **2018**, *58*, 516–523. [[CrossRef](#)]
20. Spek, A.L. checkCIF validation ALERTS: What they mean and how to respond. *Acta Crystallogr.* **2020**, *E76*, 1–11. [[CrossRef](#)]
21. Ju, Y.; Li, Z.-J.; Lu, H.; Zhou, Z.; Li, Y.; Wu, X.-L.; Guo, X.; Qian, Y.; Zhang, Z.-H.; Lin, J.; et al. Interpenetration Control in Thorium Metal–Organic Frameworks: Structural Complexity toward Iodine Adsorption. *Inorg. Chem.* **2021**, *60*, 5617–5626.
22. Liu, Y.F.; Hu, J.H.; Lee, W.T.; Yang, X.K.; Chen, J.-D. Structural transformations of cobalt (II) coordination polymers constructed from N, N'-di-3-pyridyladipoamide and tetracarboxylic acids: Disentanglement upon water coordination. *Cryst. Growth Des.* **2020**, *20*, 7211–7218. [[CrossRef](#)]
23. Bruker, A.X.S. APEX2, V2008.6, SADABS V2008/1, SAINT V7.60A, SHELXTL V6.14; Bruker AXS Inc.: Madison, WI, USA, 2008.
24. Sheldrick, G.M. Crystal structure refinement with SHELXL. *Acta Crystallogr.* **2015**, *C71*, 3–8.

Disclaimer/Publisher’s Note: The statements, opinions and data contained in all publications are solely those of the individual author(s) and contributor(s) and not of MDPI and/or the editor(s). MDPI and/or the editor(s) disclaim responsibility for any injury to people or property resulting from any ideas, methods, instructions or products referred to in the content.